MASCOT RADIOMETER DATA REVEALS SIGNS OF STRONG AQUEOUS ALTERATION OF (162173) RYUGU'S MATERIALS. M. Hamm[1,2], M. Grott[2], H. Senshu[3], J. Knollenberg[2], J. de Wiljes[4], V. E. Hamilton[5], F. Scholten[2], K. D. Matz[2], H. Bates[6,7] A. Maturilli[2], Y. Shimaki[8], N. Sakatani[9], W. Neumann[2,10], T. Okada[8], F. Preusker[2], S. Elgner[2], J. Helbert[2], E. Kührt[11,12], T.-M. Ho[13], S. Tanaka[8], R. Jaumann[1], S. Sugita[14]. [1]Freie Universität Berlin, Berlin, Germany, [2]Institute of Planetary Research, German Aerospace Center (DLR), Berlin, Germany, [3]Planetary Research and Exploration Center, Chiba Institute of Technology, Narashino, Japan, [4]Institute of Mathematics, University of Potsdam, Potsdam, Germany, [5]Southwest Research Institute, Boulder, CO USA, [6]Natural History Museum, London, UK, [7]Oxford University, Oxford, UK, [8]Institute of Space and Astronautical Science, Japan Aerospace Exploration Agency, Sagamihara, Japan, [9]Department of Physics, Rikkyo University, Toshima, Japan, [10]Klaus-Tschira-Labor für Kosmochemie, Institut für Geowissenschaften, Universität Heidelberg, Heidelberg, Germany, [11]Institute of Optical Sensor Systems, German Aerospace Center, Berlin, Germany, [12]Qian Xuesen Laboratory of Space Technology, China Academy of Space Technology, Beijing, China, [13]German Aerospace Center (DLR), Institute of Space Systems, Bremen, Germany, [14]University of Tokyo, Tokyo, Japan

Introduction: The Near-Earth Asteroid (162173) Ryugu has been investigated by the JAXA Hayabusa2 mission [1]. Hayabusa2 successfully returned samples from two sites of Ryugu's surface to Earth in December 2020. Part of this mission was the deployment of the MASCOT lander [2] which studied Ryugu's surface in detail. Ryugu is a rubble-pile asteroid covered in boulders and large pebbles [3-5]. Observations in the visible and near-infrared wavelength range indicate that Ryugu is as dark as any measured meteorite samples and that the closest match is thermally metamorphosed carbonaceous chondrites [5,6]. In the mid-infrared, the thermal infrared (TIR) instrument and the MASCOT Radiometer (MARA) revealed a high porosity of surface material of 40-50 % on average with individual boulders showing a porosity of up to 90% [7-10].

MARA observed a single boulder of the most common type on the surface of Ryugu through six channels with different filters, two broadband filters and four narrowband filters from 5.5-7 µm (B06), 8 – 9.5 µm (B08), 9.5 – 11.5 µm (B09), and 13.5 – 15.5 µm (B13). MARA thus provides the only spectrally resolved mid-infrared observations of Ryugu within the Hayabusa2 mission. Previous analysis of the MARA data was limited to the observations in the 8 – 12 µm broadband filter, which is identical to the filter used in the main spacecraft TIR instrument [9]. Here we present the analysis of the full MARA dataset and derive the variation of the emissivity within the four wavelength bands, and compare it to the spectra of carbonaceous chondrites and asteroid (101955) Bennu [11].

Thermo-Physical Parameter Estimation: We derive thermal inertia and emissivity of the surface using an Ensemble Kalman Filter data assimilation method [12] in combination with our thermal model [8]. The observation is predicted using a forward model based on a random distribution of parameters which are iteratively improved by comparing the model forecast to the MARA observation in all six channels. The forward model is a combination of a multi-scale thermal model and the instrument function. The thermal model calculates the diurnal temperature variation of each facet of a combined shape model of the boulder in front of MASCOT, incorporated into a digital elevation model of the landing site [13].

The estimated thermal inertia is 256^{+4}_{-3} J m^{-2} K^{-1} s$^{-1/2}$ which lies within the range of previous estimates and corresponds to a porosity of $46.7\ ^{+0.3}_{-0.4}$ %.

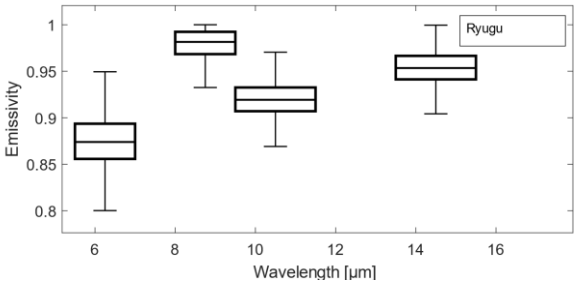

Figure 1: *Boxplot of Ryugu's emissivity estimated within the four narrowband channels of MARA. The box boundaries are given by the 25th and 75th percentile, the center is given by the median, and the whiskers are defined by outliers of the estimated distribution.*

In the four narrow bands, the emissivity is 5.5 – 7µm band to $\varepsilon_{B06} = 0.87^{+0.02}_{-0.01}$, increases within the 8 – 9.5 µm band to $\varepsilon_{B08} = 0.98^{+0.01}_{-0.01}$, decreases in the 9.5 – 11.5 µm band to $\varepsilon_{B09} = 0.92^{+0.01}_{-0.01}$, and increases again to $\varepsilon_{B13} = 0.95^{+0.02}_{-0.01}$ in the 13.5 – 15.5 µm region. These results are shown in Fig.1 where the boxplot represents the distribution of the estimated emissivity. The box boundaries are given by the 25th and 75th percentile, the center is given by the median, and the whiskers are defined by outliers within 1.5 times the interquartile range.

Comparison to Chondrite Spectra: The estimated emissivity shown in Fig. 1 are compared to laboratory spectra of carbonaceous chondrites and OTES spectra

of Bennu [14-18]. The contrast of the emissivity variation among the MARA bands is strong and much higher compared to powdered meteorite samples and more comparable to spectra of thin section samples. This contrast, is consistent with the absence of a dust layer as predicted from thermal modelling [7,19].

To compare the high-resolution laboratory spectra to the results obtained with MARA, the spectra are averaged over the instrument function of the respective instrument channels. For a systematic comparison, the averaged emissivity in the B13 and B09 bands are normalized to the B08 band, and the resulting band ratios are plotted against each other in Fig. 2. The different types of chondrites form clusters and Ryugu, Bennu, CI and CM chondrites form a common trend from which dehydrated and thermally metamorphosed chondrites differ. The group of CI chondrites are closest to Ryugu, but individual CM chondrites are also within the range of uncertainty.

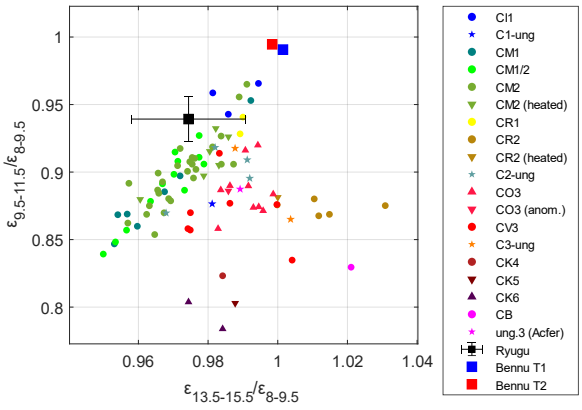

Figure 2: *Ratios of the averaged emissivity within the B09 and B13 bands, and the B08 band plotted against each other for various spectra of carbonaceous chondrite thin sections, Bennu, and Ryugu.*

Discussion: The similarity of the mid-infrared emissivity of the observed boulder to the most aqueously altered chondrites despite the strong sign of dehydration observed in the visible to near-infrared wavelength range is surprising. The loss of molecular water and OH-groups during heating occurs in steps between 200°C and 800°C while the Si-O bond structure recrystallizes at temperatures higher than 700°C [20-22]. Therefore, where the visible and near-infrared observations are sensitive to the presence of H_2O and OH-groups in the mineral, the mid-infrared is more sensitive to the structure of the Si-O bonds. Moderate temperatures, above 200°C but below 700°C could lead to the dehydration suggested by NIRS3 whereas the mid-infrared wavelength range retains the signs of past aqueous alteration. This sign for aqueous alteration in the mid-infrared observations is consistent with measurement results of Ryugu samples during initial curation processes [23,24], suggesting that mid-infrared is powerful wavelength for finding sign of aqueous alteration.

Summary: We estimate thermal inertia and spectral variation of mid-infrared emissivity of single boulder of the most common type on Ryugu by coupling a multi-scale thermal model of the boulder and the MASCOT landing site to an Ensemble Kalman Filter. Here, the full MARA data set is analyzed. A very low thermal inertia is confirmed as well as a very high overall emissivity, and the absence of a significant dust-layer. Comparing the emissivity variations among the narrowband channels to spectra of carbonaceous chondrites and Bennu reveal a similarity between Ryugu's boulders and the most aqueously altered CI and CM chondrites, supporting strong aqueous alteration occurred on Ryugu's parent body prior to any dehydration.

References:

[1] Tsuda, Y. et al. (2013), Acta Astronautica, 91, 356-362.
[2] Ho, T.-M. et al., (2021), PSS, 200, 105200
[3] Watanabe, S., et al., (2019), Science, 364, eaav8032
[4] Jaumann, R., et al., (2019), Science, 365, 817-820
[5] Sugita, S., et al., (2019), Science, 364, aaw0422
[6] Kitazato, K., et al., (2021) Nat. Astron., 5, 246-250
[7] Grott, M., et al., (2019) Nat Astron. 3, 971–976
[8] Hamm, M., et al., (2020), MNRAS, 496, 2776–2785
[9] Okada, T., et al., (2020), Nature 579, 518–522
[10] Sakatani, N., et al., (2021), Nat Astron, 5, 766-774
[11] Hamm, M., et al. (2022), Nat. Comm. https://doi.org/10.1038/s41467-022-28051
[12] Evensen, G. (2009) *Data Assimilation: The Ensemble Kalman Filter*. (Springer Science & Business Media)
[13] Scholten, F., et al., A&A 632, L5
[14] Hamilton, V. E., et al., (2021), A&A 650, A120
[15] Bates, H., et al., (2020), MAPS. 55, 77–101
[16] Bates, H., et al., (2021), JGR: Planets 126, e2021JE006827
[17] Beck, P., et al., (2018), Icarus 313, 124–138
[18] Maturilli, A., et al., (2016), Earth Planet Sp., 68, 113
[19] Biele, J., et al., PEPS, 6, 48
[20] King, A., et al., (2015), Earth Planet Sp 67, 198
[21] King, A., et al., (2021), GCA 298, 167–190
[22] Alemanno, G., et al., EPSL546, 116424
[23] Yada, T. et al. (2021) Nat. Astron. https://doi.org/10.1038/s41550-021-01550-6
[24] Pilorget, C. Et al. (2021) Nat. Astron. https://doi.org/10.1038/s41550-021-01549-z.